Photo-induced refraction of nanoparticulate organic-inorganic TiO_2-pHEMA hybrids

Andrii Uklein, Pavlo Gorbovyi, Mamadou Traore, Luc Museur, Andrey Kanaev

Photo-induced refraction of nanoparticulate organic-inorganic TiO_2-pHEMA hybrids

Andrii Uklein,[1,2] Pavlo Gorbovyi,[3] Mamadou Traore,[3] Luc Museur,[1*] Andrey Kanaev[3]

[1] *Université Paris 13, Sorbonne Paris Cité, Laboratoire de Physique des Lasers, CNRS UMR 7538, F-93430, Villetaneuse, France*
[2] *National Academy of Sciences Institute of Physics, Kiev 03680 Ukraine*
[3] *CNRS, UPR 3407, LSPM, Université Paris 13, Sorbonne Paris Cité, F-93430, Villetaneuse, France*
[*] luc.museur@univ-paris13.fr

Abstract: We report on photoinduced modifications of the refractive index of nanoparticulate TiO_2-pHEMA organic-inorganic hybrids. The samples with titania concentration ranging from $0.88 \cdot 10^{20}$ to $17.6 \cdot 10^{20}$ cm^{-3} were irradiated and analyzed with UV light at 375 nm. A reduction of the refractive index is observed in all samples. Although the photoinduced refraction was stronger in samples with higher titania concentration, its normalized value per Ti^{3+} center $a_0 = -2.4 \cdot 10^{-23}$ cm^3 remained constant. The change of refractive index correlates with the material photochromic response due to the accumulation of polaronic Ti^{3+} centers in the material.

OCIS codes: (160.4670) Optical materials; (160.4760) Optical properties; (160.5320) Photorefractive materials; (160.4236) Nanomaterials.

References and links

1. P. Gómez-Romero and C. Sanchez, eds. *Functional Hybrid Materials*. (Wiley-VCH Verlag GmbH & Co., 2003).
2. L. Nicole, L. Rozes, and C. Sanchez, "Integrative Approaches to Hybrid Multifunctional Materials: From Multidisciplinary Research to Applied Technologies," Advanced Materials, **22**(29), 3208-3214 (2010).
3. C. Sanchez, P. Belleville, M. Popall, and L. Nicole, "Applications of advanced hybrid organic-inorganic nanomaterials: from laboratory to market," Chemical Society Reviews, **40**(2), 696-753 (2011).
4. R. Houbertz, G. Domann, C. Cronauer, A. Schmitt, H. Martin, J.U. Park, L. Fröhlich, R. Buestrich, M. Popall, U. Streppel, P. Dannberg, C. Wächter, and A. Bräuer, "Inorganic–organic hybrid materials for application in optical devices," Thin Solid Films, **442**(1–2), 194-200 (2003).
5. R. Reisfeld, A. Weiss, T. Saraidarov, E. Yariv, and A.A. Ishchenko, "Solid-state lasers based on inorganic–organic hybrid materials obtained by combined sol–gel polymer technology," Polymers for Advanced Technologies, **15**(6), 291-301 (2004).
6. D.J. Kang and B.-S. Bae, "Photo-imageable Sol–Gel Hybrid Materials for Simple Fabrication of Micro-optical Elements," Accounts of Chemical Research, **40**(9), 903-912 (2007).
7. R.A.S. Ferreira, P.S. André, and L.D. Carlos, "Organic–inorganic hybrid materials towards passive and active architectures for the next generation of optical networks," Optical Materials, **32**(11), 1397-1409 (2010).
8. K. Tanaka and K. Shimakawa, "Chalcogenide glasses in Japan: A review on photoinduced phenomena," physica status solidi (b), **246**(8), 1744-1757 (2009).
9. S. Ducharme, J. Hautala, and P.C. Taylor, "Photodarkening profiles and kinetics in chalcogenide glasses," Physical review B, **41**(17), 12250-12259 (1990).
10. A.I. Kuznetsov, O. Kameneva, N. Bityurin, L. Rozes, C. Sanchez, and A. Kanaev, "Laser-induced photopatterning of organic–inorganic TiO 2-based hybrid materials with tunable interfacial electron transfer," Physical Chemistry Chemical Physics, **11**(8), 1248-1257 (2009).
11. O. Kameneva, A.I. Kuznestov, L.A. Smirnova, L. Rozes, C. Sanchez, A. Alexandrov, N. Bityurin, K. Chhor, and A. Kanaev, "New photoactive hybrid organic-inorganic materials based on titanium-oxo-PHEMA nanocomposites exhibiting mixed valence properties," Journal of Materials Chemistry, **15**(33), 3380-3383 (2005).
12. E. Fadeeva, J. Koch, B. Chichkov, A. Kuznetsov, O. Kameneva, N. Bityurin, C. Sanchez, and A. Kanaev, "Laser imprinting of 3D structures in gel-based titanium oxide organic-inorganic hybrids," Applied Physics A: Materials Science & Processing, **84**(1), 27-30 (2006).

#180200 - $15.00 USD Received 2 Jan 2013; revised 7 Feb 2013; accepted 7 Feb 2013; published 1 Apr 2013

13. P. Gorbovyi, A. Uklein, S. Tieng, O. Brinza, M. Traore, K. Chhor, L. Museur, and A. Kanaev, "Novel nanostructured pHEMA-TiO2 hybrid materials with efficient light-induced charge separation," Nanoscale, **3**(4), 1807-1812 (2011).
14. N. Bityurin, A.I. Kuznetsov, and A. Kanaev, "Kinetics of UV-induced darkening of titanium-oxide gels," Applied Surface Science, **248**(1-4), 86-90 (2005).
15. L. Museur, P. Gorbovyi, M. Traore, A. Kanaev, L. Rozes, and C. Sanchez, "Luminescence properties of pHEMA-TiO2 gels based hybrids materials," Journal of luminescence, **132**(5), 1192-1199 (2012).
16. A. Zakery and S.R. Elliott, "Optical properties and applications of chalcogenide glasses: a review," Journal of Non-Crystalline Solids, **330**(1-3), 1-12 (2003).
17. Mehta, "Applications of chalcogenide glasses in electronics and optoelectronics: A review," Journal of Scientific & Industrial Research, **65**(10), 777-786 (2006).
18. Q. Zhan and J.R. Leger, "Microellipsometer with Radial Symmetry," Appl. Opt., **41**(22), 4630-4637 (2002).
19. K. Fedus and G. Boudebs, "Determination of photo-induced changes in linear optical coefficients by the Z-scan technique," J. Opt. Soc. Am. B, **26**(11), 2171-2175 (2009).
20. M. Sheik-Bahae, A.A. Said, T.H. Wei, D.J. Hagan, and E.W. Van Stryland, "Sensitive measurement of optical nonlinearities using a single beam," Quantum Electronics, IEEE Journal of, **26**(4), 760-769 (1990).
21. A. Afanasiev, A. Alexandrov, N. Agareva, N. Sapogova, L. Smirnova, and N. Bityurin. "UV induced of linear and non-linear IR optical properties of dielectrics for photonic applications," presented in *FLAMN-10*, St. Petersburg, Russia. 2010
22. V. Gayvoronsky, S. Yakunin, V. Nazarenko, V. Starkov, and M. Brodyn, "Techniques to Characterize the Nonlinear Optical Response of Doped Nematic Liquid Crystals," Molecular Crystals and Liquid Crystals, **426**(1), 231-241 (2005).
23. J.U. Park, W.S. Kim, and B.S. Bae, "Photoinduced low refractive index in a photosensitive organic–inorganic hybrid material," J. Mater. Chem., **13**(4), 738-741 (2003).
24. B.R. Bennett, R.A. Soref, and J.A. Del Alamo, "Carrier-induced change in refractive index of InP, GaAs and InGaAsP," Quantum Electronics, IEEE Journal of, **26**(1), 113-122 (1990).
25. N.A. Deskins and M. Dupuis, "Electron transport via polaron hopping in bulk TiO_{2}: A density functional theory characterization," Physical review B, **75**(19), 195212 (2007).
26. R. Ulbricht, E. Hendry, J. Shan, T.F. Heinz, and M. Bonn, "Carrier dynamics in semiconductors studied with time-resolved terahertz spectroscopy," Reviews of Modern Physics, **83**(2), 543-586 (2011).
27. R.G. Hunsperger, *Integrated Optics*. 2009, Springer New York: New York.
28. Tanaka Keiji, "Photo-induced phenomena in chalcogenide glass: Comparison with those in oxide glass and polymer," Journal of Non-Crystalline Solids, **352**(23-25), 2580-2584 (2006).
29. A. Ljungstrom and T. Monro, "Observation of light-induced refractive index reduction in bulk glass and application to the formation of complex waveguides," Opt. Express, **10**(5), 230-235 (2002).
30. L. Merhari, *Hybrid nanocomposites for nanotechnology: electronic, optical, magnetic and biomedical applications*. 2009: Springer Verlag.

1. Introduction

Organic-inorganic hybrids have deserved a growing interest last decade owing to a combination of useful properties of their constituting components [1, 2]. The flexibility and shaping versatility of an organic polymer and high refractive index of an inorganic component permit considering the hybrids materials for many potential applications in field of photonics [3-7]. Among these materials, the TiO_2-based hybrids are of particular interest because of their efficient photodarkening at the exposition to photons with energy above that of the band gap ($h\nu \geq 3.25$ eV). Conversely to the well-known chalcogenide glasses [8, 9], which also exhibit photodarkening, the bleaching of the dark domains in hybrids can be photoinduced, without need of the annealing process [10]. Reversible photopatterning of these optically transparent materials makes them potentially suitable for 2D/3D laser structuring.

Previously, we have reported on the elaboration of TiO_2 gel-based hybrids including macroscopic interpenetrating inorganic oxo-titanate, and organic poly(hydroxethyl methacrylate) pHEMA, networks [11]. These nanocomposites, obtained without shrinkage, show high transparency and mechanical stability, allowing optical-grade surface polishing, as well as high photonic sensitivity, which permit realization of 3D microstructures using femtosecond lasers [11, 12]. The photodarkening of the pHEMA-TiO_2 hybrids results from an efficient charges separation at the organic-inorganic interface. Actually, the conduction-band (CB) electron remains localized onto the inorganic component as small polaron-like Ti^{3+} center, whereas the valence-band (VB) hole leaves to the polymer component. The localysed

#180200 - $15.00 USD Received 2 Jan 2013; revised 7 Feb 2013; accepted 7 Feb 2013; published 1 Apr 2013

electron is responsible of the material absorption in the visible spectral range according to the process $Ti^{3+} + h\nu(VIS) \rightarrow Ti^{4+} + e^{-}(CB)$. Recently, nanoparticulate pHEMA-TiO_2 hybrids with nanoscale morphology control and record charge separation efficiency (50%) have been realized [13]. The relevant physical mechanisms involved in the photodarkening have been previously discussed in Refs [10, 14, 15].

Because of the Kramers-Kroning relation, changes of the transmission in photochromic materials usually lead to the modification of their refraction properties. The photoinduced modifications may enable fabrication of optoelectronic devices as Bragg gratings or waveguides [16, 17]. In order to optimize the optical writing process, accurate measurements of photoinduced modifications of the linear refraction coefficient have to be performed. Practically, the absorption modifications are probed by transmission measurements, whereas the variations of refractive index are usually measured by microellipsometry [18] and/or Z-scan methods [19, 20]. First attempts to measure the photoinduced refraction in the gel-based TiO_2 organic-inorganic hybrids were recently presented by Bityurin's group using the phase grating method [21], who reports positive refraction changes of $+1.6x10^{-24}$ cm^3 per Ti^{3+} center at 1570 nm. The obtained value can be assigned to bound electrons, since free electrons produce negative contribution to the refraction. More experiments are required to verify the refraction changes in the photochromic hybrids.

In this publication we report on the photoinduced refraction measurements in novel nanoparticulate TiO_2-pHEMA organic-inorganic hybrids with an improved photochromic response in the UV spectral range. The article is organized as follow: the experimental setup and sample preparation procedure are described in section 2. The theoretical formalism of the refractive index calculations is briefly presented in section 3. The experimental results and discussion of the photoinduced refractive index are given in section 4.

2. Experiment

The measurements were performed by using an original approach developed by Gayvoronsky et al. [22]. This approach has some similarities with the well-known z-scan method, however in contrast to it the sample is kept in a fixed position. Actually, the hybrid samples are irradiated with TEM_{00} Gaussian shape laser beam. The modifications of the absorption coefficient $\Delta\alpha$ and refractive index Δn depend on the laser dose and, at least for small doses, the spatial distributions of $\Delta\alpha$ and Δn are of similar Gaussian shape. Depending on the sign of Δn, the induced phase shift results in a self-focusing ($\Delta n>0$) or a self-defocusing ($\Delta n<0$) of the laser beam. The modifications on the beam divergence are probed by measurements of the sample normalized transmittance through a small circular aperture placed on the beam propagation axis in the far field. The refractive index variations can be obtained by fitting the experimental points with theoretical expression of the on-axis transmittance in the Gaussian beam approximation.

Table 1: Hybrid samples characteristics: $[Ti^{4+}]$ concentration, thickness (L), quantum yield η_a, photoinduced refractive index change Δn_0, density of $[Ti^{3+}]$ centers and refractive index modification per Ti^{3+} center a_0. All values are given for a reference irradiation dose equal to 10 J/cm^2.

	$[Ti^{4+}]$ $10^{20}cm^{-3}$	L μm	η_a %	Δn_0 10^{-4}	$[Ti^{3+}]$ 10^{18} cm^{-3}	a_0 10^{-23} cm^3
X1	0.88	94.9	14.5	- 0.23	0.90	-2.55
X2	1.76	78;1	13.4	- 0.36	1.72	-2.13
X5	4.4	92.9	7.0	-0.48	2.59	-2.17
X10	8.8	98.6	16.5	- 2.42	10.85	-2.23
X20	17.6	82.7	15.1	- 5.64	19.01	-2.97

#180200 - $15.00 USD Received 2 Jan 2013; revised 7 Feb 2013; accepted 7 Feb 2013; published 1 Apr 2013

The general synthesis scheme adopted for hybrids fabrication is described in details in ref [13]. Briefly, the titania based hybrids samples are synthetized in a three step process. Firstly, monodispersed titanium-oxo-alkoxy nanoparticles of size 5.2 nm are generated in 2-propanol solvent in a sol-gel reactor with rapid micromixing. On the second step, the solvent replacement by HEMA results in ligands exchange at the nanoparticles surface, and leads to the stable nanoparticulate precursor in a HEMA solution. On this stage, the concentration of the inorganic component is adjusted. Finally, the precursor solution is filled between two microscope plates and thermally polymerized. Five samples with different titanium oxide concentrations, 0.88×10^{20} (x1), 1.76×10^{20} (x2), 4.4×10^{20} cm^{-3} (x5), 8.8×10^{20} (x10) and 17.6×10^{20} cm^{-3} (x20) were prepared. The samples thicknesses were carefully measured with optical microscope in the cross-section of the irradiated zone. The characteristics of all samples are reported in Table 1. Additionally, a reference pHEMA polymer sample has been prepared.

The experimental setup used for measurements of the absorption and refraction kinetics is shown in Fig. 1. A UV laser diode at 375 nm (from Oxxius) with a single mode fiber output delivers, after spatial filtering and collimation, a TEM_{00} beam of 0.5 mW cw power after spatial filtering system (SFS) and collimation. This beam interacts with the sample at normal incidence, and the transmitted beam is analyzed by two photodiodes (D1 and D2). A beam splitter (Sp), positioned immediately after the sample, reflects a small part of the beam to photodiode D1, which monitors the total transmitted power. A wide aperture lens (L), positioned as close as possible to the beam splitter (Sp), was used to collect the transmitted light. The photodiode D2 measures the transmitted power through a small diaphragm ($r_a = 225\,\mu m$) placed in far field and monitors the convergence/divergence of the beam due to the photoinduced refractive index variations in the sample. The sample is placed at the position z_s after the beam waist that was found at the position z_w from the SFS. The distance between the sample and diaphragm is $d = 60\,cm$ and the typical intensity of 280 mW/cm^2 has been used to irradiate the samples.

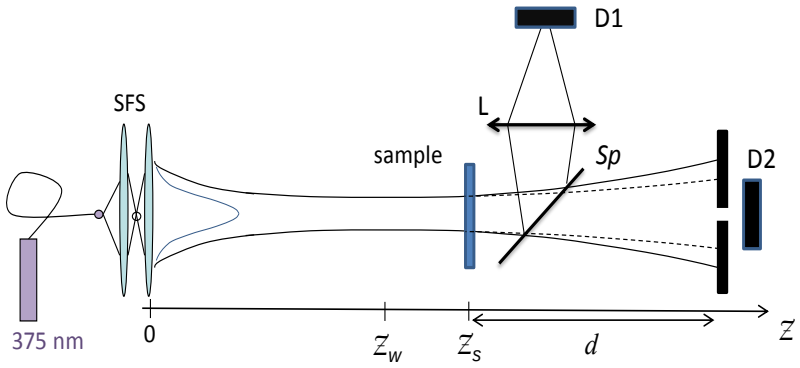

Fig. 1: Experimental setup: SFS – spatial filtering system, Sp is a beam splitter, S - sample, D1 and D2 are photodiodes. The beam waist position is taken as the origin of the axis *z*.

The experimental results analysis was based on the Gaussian-shape beam approximation. Consequently, the spatial profile of the UV laser beam after the spatial filtering was carefully measured using a CCD beam analyzer at different distances from the source. The measured beam square radius $w^2(z)$ (half width at $1/e^2$ on intensity) as function of the propagation is plotted in Fig. 2(a). This variation can be fitted with the usual expression

#180200 - $15.00 USD Received 2 Jan 2013; revised 7 Feb 2013; accepted 7 Feb 2013; published 1 Apr 2013

$w(z) = w_0\sqrt{1+(z/z_0)^2}$, where $z = Z - Z_w$ and $z_0 = \pi w_0^2/\lambda$ (Rayleigh range). An excellent agreement has been found with the fit parameters $Z_w = 28.7\,cm$ and $w_0 = 173\,\mu m$ (beam waist). The spot size at the sample plane that correspond to obtained parameters magnitudes is similar to the one measured directly by CCD beam analyzer $w \approx 200\,\mu m$. Additionally, we have checked the Gaussian profiles of the photodarkened domains. An example of such photodarkened area, observed with an optical microscope, is shown on the Fig. 2(b). We have superimposed on this picture, the absorption profile obtained with the CCD camera when the sample is illuminated with a white light. According to the displayed profiles cross-sections, the distribution of the photoinduced modifications at the irradiated area is Gaussian. Next we describe the formalism used for the experimental data analysis.

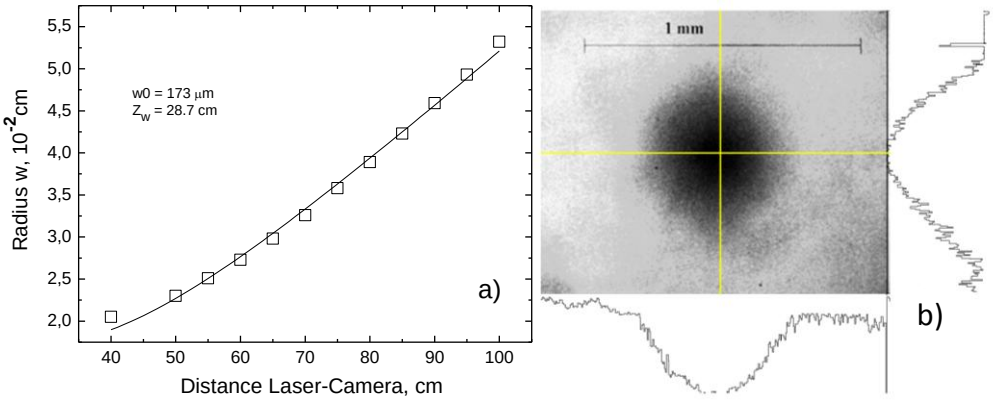

Fig. 2: a) Evolution of square beam radius (half width at $1/e^2$) along the propagation (Z axis). The full line is a fit with the usual expression of $w(z)$ for Gaussian beams (see text). b) Image of the darkened area of sample x10 and spatial variation of the sample transmission.

3. Theoretical formalism of the refraction measurements

Assuming a Gaussian beam propagating along the $+z$ direction and the coordinate origin being at the Gaussian beam waist, the electric field incident on the sample is written:

$$E_e(r,z) = E_0\frac{w_0}{w(z)}\exp\left[-\frac{r^2}{w^2(z)} - i\frac{kr^2}{2R(z)}\right]\exp\left[-i\phi(z)\right] \quad (1)$$

where E_0 denotes the on-axis electric fields amplitude, r is the radial coordinate, z is the sample position and $R(z) = z\left[1+(z_0/z)^2\right]$ stands for the wave front radius of curvature. The phase term $\phi(z)$ contains all the radially uniform phase variations. The sample is considered as thin with a thickness L smaller than the Rayleigh range ($L < z_0$). Consequently, any changes of the laser beam profile induced by linear diffraction phenomena can be neglected, which was experimentally supported by the propagating beam analysis. Moreover, we suppose that (i) photoinduced modifications are uniform in the direction z of the beam propagation inside the sample and (ii) their radial distribution corresponds to the spatial profile of the beam intensity at the sample position $z = z_S$. Thus, we can write:

#180200 - $15.00 USD Received 2 Jan 2013; revised 7 Feb 2013; accepted 7 Feb 2013; published 1 Apr 2013

$$\Delta n(r,D) = \Delta n_0(D)\exp\left[-\frac{2r^2}{w^2(z_S)}\right]$$
$$\Delta \alpha(r,D) = \Delta \alpha_0(D)\exp\left[-\frac{2r^2}{w^2(z_S)}\right] \quad (2)$$

where Δn_0 and $\Delta \alpha_0$ are respectively photoinduced variations of the on-axis refractive index and absorption coefficients and *D* is the irradiation dose.

In general case, one has to explicitly consider the beam propagation inside the absorbing medium. However the above suppositions allow simplifying the modeling. For a relatively thin sample and low absorbance, one can neglect changes of the spatial beam shape and absorbance along the z-axis. We consider that the i-th laser pulse propagates in the medium prepared by the i-1 previous pulses, which induce an absorbing area with the absorption coefficient $\alpha+\Delta\alpha_0(D_{i-1})$ of the Gaussian spatial shape in (*x*,*y*) plane and independent on z coordinate within the sample. In these conditions, the electric field at exit surface of the sample than be expressed by:

$$E_s(r,z,D) = E_e(r,z)\exp\left[-\alpha L/2\right]\exp\left[-\left(i\Delta\phi_0 + \frac{\Delta\alpha_0 L}{2}\right)\exp\left(-\frac{2r^2}{w^2(z_S)}\right)\right] \quad (3)$$

where α is the absorption coefficient of the non-irradiated sample (*D=0*) and $\Delta\phi_0 = 2\pi\Delta n_0 L/\lambda$ is the photoinduced phase shift. To calculate the amplitude of the electric field in the plane of the aperture, we use the Gaussian decomposition method described in Ref. [20]. The electric field at the output of the sample is decomposed as a series of Gaussian beams with different waists and wave front curvatures. Each individual Gaussian beam is then propagated independently along the *z* axis in the free space. The electric field $E_a(r,z'=z+d,D)$ in the receivers' aperture plane is obtained after summing up all the individual beams. Thus:

$$E_a(r,z'=z+d,D) = E_e(r=0,z)e^{-\alpha L/2}\sum_{m=0}^{\infty}(-1)^m\frac{\left(i\Delta\phi_0+\frac{\Delta\alpha_0 L}{2}\right)^m}{m!}\frac{w_{m0}}{w_m}\exp\left(-\frac{r^2}{w_m^2}\right)\exp i\left(-\frac{kr^2}{2R_m}+\theta_m\right) \quad (4)$$

where *d* is the distance between the sample and the aperture plane. The other geometry defined parameters are [20]:

$$w_{m0}^2 = w^2(z)/(2m+1),\quad d_m = kw_{m0}^2/2,\quad R_m^2 = d\left[1-g/\left(g^2+d^2/d_m^2\right)\right]^{-1}$$
$$\theta_m = \tan^{-1}\left[\left(d/d_m\right)/g\right],\quad w_m^2 = w_{m0}^2\left(g+d^2/d_m^2\right)\ \text{and}\quad g = 1+d/R(z)$$

The Eq. (4) describes sufficiently thin and low absorbing samples. With an increase of both thickness and absorbance, the deviation from Eq. (4) appears. This deviation between the experiment and modeling will be considered as a criterion of the above formalism applicability.

Finally, we define the normalized on-axis transmittance:

#180200 - $15.00 USD Received 2 Jan 2013; revised 7 Feb 2013; accepted 7 Feb 2013; published 1 Apr 2013

$$T(D) = \frac{P_{on\,axis}}{P_{total}} = \frac{\int_0^{r_a} \left|E_a(r,z,D)\right|^2 r\,dr}{\int_0^{\infty} \left|E_a(r,z,D)\right|^2 r\,dr} \quad (5)$$

where r_a is the aperture radius. This normalization Eq. (5) permits distinguishing the refraction component of the field variation on the beam propagating in an absorbing medium. Experimentally, the powers $P_{on\text{-}axis}$ and P_{total} are measured separately, and the photoinduced variation of refractive index $\Delta n_0(D)$ is obtained by fitting the experimental normalized on-axis transmittance with the theoretical expression of $T(D)$ given by Eq. (5).

4. Results and discussion

It's worth to notice that the usual Z-scan approach is not appropriate for measurements of the refraction modifications in materials with high sensitivity to photodarkening and long relaxation. Indeed, consistent Z-scan traces necessary for measurement of $\Delta n_0(D)$ at a given irradiation dose *D* require a fresh zone of the sample to be irradiated for each position Z. This needs in turn a complicated optical alignment, which would assure no axial beam deviation and conservation of laser dose during the lateral (*r*) and longitudinal (*Z*) sample displacements. The method proposed in the present article, allows to measure $\Delta n_0(D)$ with a large range of irradiation doses in the same experimental geometry. Moreover, its sensitivity is high. In our experimental conditions, as we will show, we were able to measure variations of 1% of the normalized on-axis transmittance. Taking into account the diaphragm radius ($r_a = 225\mu m$) this corresponds to a phase shift $\left|\Delta\phi_0\right| \approx 33mrad$. Consequently, the minimum measurable optical path length variation is $\Delta n_0 L = \Delta\phi_0 \lambda / 2\pi \approx \lambda / 190$.

The UV irradiation of pHEMA/TiO_2-based hybrids materials induces modifications of both absorption coefficient and refractive index. The total and on-axis transmittances, as a function of the UV irradiation dose, are shown in Fig. 3(a) and 3(b) respectively. In the same experimental conditions, the transmittance of the pure pHEMA reference sample is found unaffected by the irradiation, which evidence that the effect is entirely due the presence of the inorganic TiO_2 component. Since, the measured changes in the refraction $\Delta n_0(D)$ correlate with the photodarkenning of the sample, we will first discuss the photoinduced modifications of total absorption coefficient $\Delta\alpha_0(D)$ (Fig. 3(a)). For the sake of simplicity, we mainly present next parts the results obtained in samples X1 and X10. A similar procedure has been used to measure $\Delta\alpha_0(D)$ and $\Delta n_0(D)$ in others samples.

In pHEMA/TiO_2-based hybrids materials, the darkening is assigned to Ti^{+3} centers [10, 11] which are formed by the CB electron trapping on Ti^{4+} after photoexcitation below 380 nm ($h\nu \geq E_g = 3.2\ eV$). The scheme of the relevant processes involved in the Ti^{3+} centers formation is drawn in the Fig. 4. The absorption of a photon $h\nu$ results in the electron transition from the valence band, due to O^{2-} *2p* orbital, to the conduction band, due to Ti^{4+} *3d* orbital. Whereas the hole is supposed to escape rapidly into the organic pHEMA component, the remaining CB electron is trapped into the inorganic component with the quantum efficiency η_a. The spontaneous relaxation of the photoinduced charges is slow resulting in a Ti^{3+} centers lifetime of several weeks [10]. On the other hand, the maximal concentration of the Ti^{3+} centers is limited by the inner-photoeffect, which corresponds to the trapped electrons excitation. The successfully reexcited electrons can leave the inorganic component, and

#180200 - $15.00 USD Received 2 Jan 2013; revised 7 Feb 2013; accepted 7 Feb 2013; published 1 Apr 2013

recombine with holes localized in the organic component. This last process is characterized by the quantum efficiency η_b. Accordingly, the rate equation of Ti^{3+} concentration is:

$$\frac{d[Ti^{3+}]}{dt} = -\left(\eta_a \sigma_a + \eta_b \sigma_b\right).[Ti^{3+}].\frac{I}{h\nu} + \eta_a \sigma_a [Ti^{4+}]_0.\frac{I}{h\nu} \quad (6)$$

where $\sigma_a = 4.3\ 10^{-21}$ cm^2 and $\sigma_b = 6\ 10^{-19}$ cm^2 accounts for the absorption cross sections of respectively Ti^{4+} and Ti^{3+} at 375 nm [10], $[Ti^{4+}]_0$ is the initial density of titania, and I is the laser intensity in W/cm^2. The evolution of Ti^{3+} concentration as a function of the irradiation dose D can be obtained from the previous expression:

$$[Ti^{3+}] = \frac{[Ti^{4+}]_0}{1 + \frac{\eta_b \sigma_b}{\eta_a \sigma_a}}.\left(1 - \exp\left(\frac{-\left(\eta_a \sigma_a + \eta_b \sigma_b\right)}{h\nu}.D\right)\right) \quad (7)$$

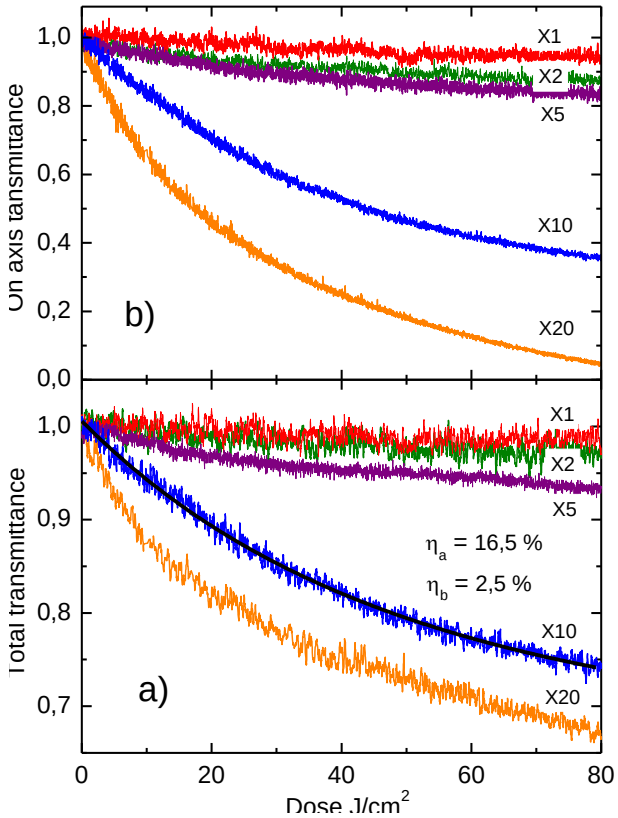

Fig. 3: Variation of total transmittance (a) and on-axis transmittance (b) in the hybrid samples as a function of UV irradiation dose. The dark solid line represents the fit of the experimental transmittance of sample X10 by Eq. (9) with parameters η_a = 16.5%, η_b =2.5 %.

The kinetics of the total transmittance at 375 nm is plotted in the Fig. 3(a) as a function of the UV irradiation dose for all hybrids samples. As expected, the absorption increases both with the titania concentration and UV irradiation dose. According to the model discussed

#180200 - $15.00 USD Received 2 Jan 2013; revised 7 Feb 2013; accepted 7 Feb 2013; published 1 Apr 2013

above and the assumption about the absorption coefficient uniformity along the z direction proposed in section 3, the transmittance curves can be described by the usual Beer-Lambet law, assuming that each produced Ti^{3+} center replaces one Ti^{4+}:

$$T = \frac{P_{total}(D)}{P_{total}(D=0)} \propto \exp\left(-(\sigma_b - \sigma_a)\left[Ti^{3+}\right]L\right) \quad (8)$$

where L is the sample thickness and the density $[Ti^{3+}]$ is given by Eq. (7). The quantum efficiencies η_a and η_b involved in the calculation of $[Ti^{3+}]$ are free parameters which can be obtained from the fit of the experimental data by Eqs. (8) and (9). The theoretical transmission curve of sample X10, is plotted by dark solid line in Fig. 3(a). An excellent agreement with the experimental curve supports the approximation of a uniform distribution of the absorbing species along the laser beam propagation. The obtained quantum efficiencies η_a for the charge separation process are ranging from 13.5% to 16.5% excepted for the sample X5 for which $\eta_a = 7\%$. A less efficient polymerization in sample X5 may account for this difference. The quantum efficiency η_b of the inner photoeffect process is ranging from 1.5% to 2.5% for all samples. The values of η_a are reported in Table 1. It's worth to remark that the obtained charges separation efficiency is considerably smaller than that measured with photoexcitation at 355 nm ($\eta_a \approx 50\%$) [13]. This may be explained by the activation barrier that the photoinduced hole has to overcome in order to escape the inorganic component. The holes remained into the inorganic component likely recombine with the CB electrons with the probability 1-η_a .

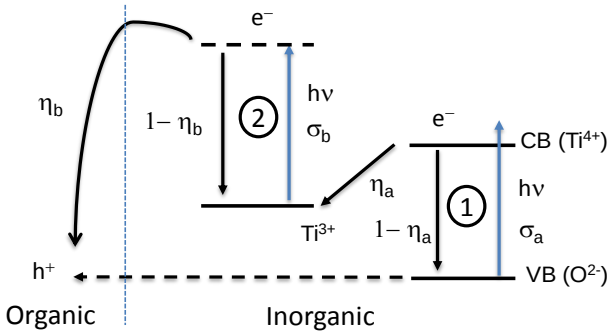

Fig. 4: Scheme of the relevant processes involved in the photodarkenning of pHEMA-TiO_2 hybrids materials.

The photoinduced modifications of the absorption coefficient $\Delta\alpha_0 = (\sigma_b - \sigma_a)[Ti^{3+}]$ are proportional to the number density of localized electrons $[Ti^{3+}]$ and cross sections difference. The number density $[Ti^{3+}]$ is calculated using quantum efficiencies η_a and η_b obtained from the fit of total transmittance curves with Eqs. (8) and (8).

With knowledge of the total sample transmittance, the on-axis transmittance provides information about modifications of the refractive index. In the present experiment, the normalized on-axis transmittance *T(D)* decreases with the UV irradiation dose in all hybrid samples as shown in Fig. 3(b). This reduction of on-axis transmittance corresponds to the negative variations of the refractive index ($\Delta n_0 < 0$), since the samples were positioned after the beam waist.

#180200 - $15.00 USD Received 2 Jan 2013; revised 7 Feb 2013; accepted 7 Feb 2013; published 1 Apr 2013

The experimental data permit evaluation of the photoinduced refractive index according to the formalism described in section 3. The fits of the normalized on-axis transmittance of samples X1 and X10 by Eq. (5) are plotted as dash curves in Fig. 5(b). In these fits the refractive index modification $\Delta n_0(D)$ is supposed to vary linearly with the Ti^{3+} concentration $\Delta n_0 = a_0 \cdot [Ti^{3+}]$. Consequently, the only free parameter in the Eq. (5) is the factor a_0 which represents the refractive index variation per Ti^{3+} center. An excellent agreement with the experiment is obtained for sample X1 in the whole range of laser doses $0 < D < 60$ J/cm^2. On the other hand, the normalized on-axis transmittance of sample X10 can be satisfactory fitted by Eq. (5) in a restricted range of laser doses $0 < D < 20$ J/cm^2 responsible for the linear regime of the photodarkening. As discussed in section 3, the total sample absorption of ≤10% (see Fig. 3) sets limit of applicability of the proposed formalism. This is in agreement with Ref. [20], where non-linear absorption in optical media has been considered.

The variations of the refractive index $\Delta n_0(D)$ of samples X1 and X10 are reported in Fig. 5(a). Typical values $\Delta n_0 \approx -0.67 \cdot 10^{-4}$ in sample X1 at $D = 60$ J/cm^2 and $\Delta n_0 \approx -4 \cdot 10^{-4}$ in sample X10 at $D = 20$ J/cm^2 were obtained.

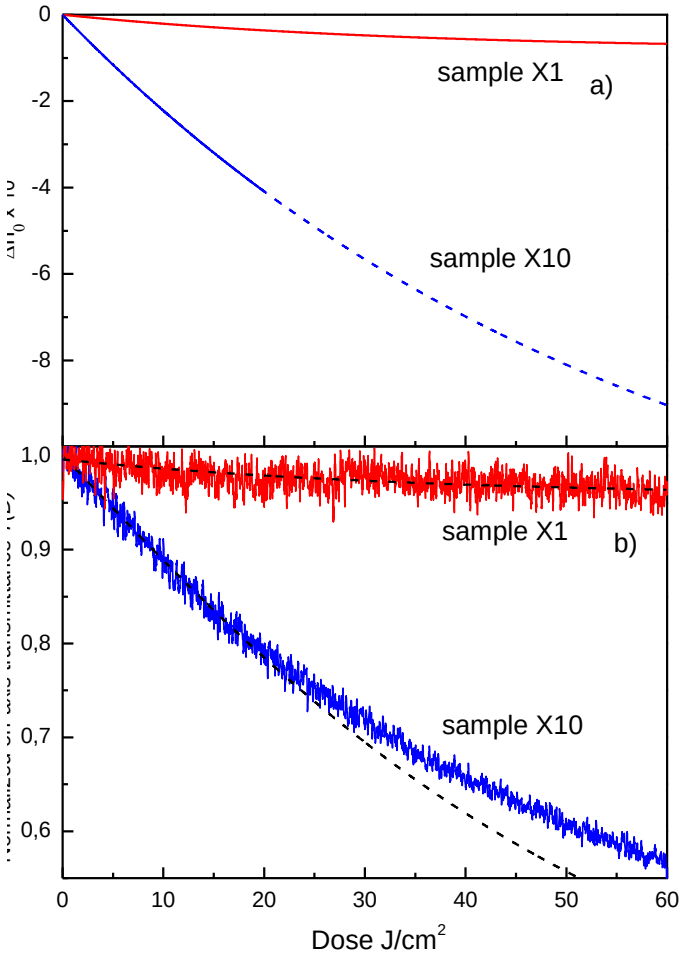

#180200 - $15.00 USD Received 2 Jan 2013; revised 7 Feb 2013; accepted 7 Feb 2013; published 1 Apr 2013

Fig. 5: Variations of refractive index Δn_0 (a) and normalized on-axis transmittance (b) of hybrid samples X1 and X10 versus the UV irradiation dose. On (b) the dashed lines represent the fits of on axis transmittance by Eq. (5).

The proposed method of the refractive index variation measurements is valid in the Gaussian phase shift approximation when both distributions of $\Delta n(r,D)$ and $\Delta\alpha(r,D)$ reproduce the Gaussian spatial profile of the laser beam. Indeed, due to the saturation of the Ti^{3+} concentration, the $\Delta n(r,D)$ profile becomes progressively flat when the irradiation dose increases. Experimentally, this results in a decrease of the photoinduced divergence and an underestimation of the normalized on-axis transmittance calculated by the Eq. (5). This effect is observed in the sample X10 when $D > 20$ J/cm^2. For this reason, we were unable to calculate the refractive index changes in the range of a strong material darkening. However, to have an idea about the refractive index modification in sample X10 at higher doses, we have plotted the expected variation of $\Delta n_0(D)$ as a dot line in Fig. 5(a). A pure numerical approach allowing calculating the electric field $E_a(r,z,D)$ in the aperture plane and taking into account real modifications of the $\Delta n(r,D)$ profile is currently under consideration in our group. This should allow measuring the refractive index modification beyond the Gaussian phase shift approximation.

The refractive index $\Delta n_0(D)$ modifications have been measured in samples X2, X5 and X20 using the above described procedure. For the sake of comparison, we report in Table 1 the values of $\Delta n_0(D)$ measured in all samples for the same reference irradiation dose $D \approx 10 J/cm^2$. As expected because of a stronger absorbance, $\Delta n_0(D)$ increases with the titania concentration in the hybrid samples. To account for the increased number of the photoinduced centers, the photoinduced refraction can be normalized on their number density. The relevant density of the photoinduced Ti^{3+} centers for the reference dose together with the refractive index variation per Ti^{3+} center $a_0 = \Delta n_0 / [Ti^{3+}]$ are also reported in Table 1. As Fig. 6 shows, this parameter appears to be almost independent on the titania concentration in the considered samples. Its mean value $a_0 \approx -2.4 \cdot 10^{-23} cm^3$ is indicated by a dot line in Fig. 6.

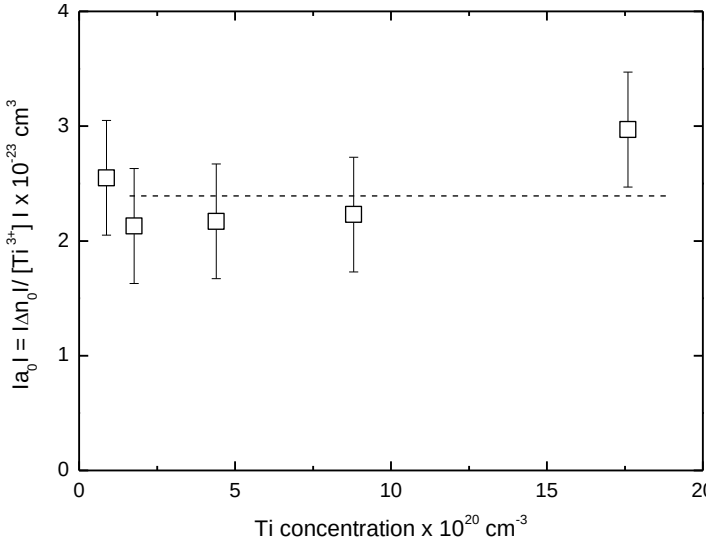

#180200 - $15.00 USD Received 2 Jan 2013; revised 7 Feb 2013; accepted 7 Feb 2013; published 1 Apr 2013

Fig. 6: Photoinduced refractive index modification per Ti^{3+} center $a_0 = \Delta n_0 / \left[Ti^{3+} \right]$.

For the experimental viewpoint, the refractive index modification results from the photoexcitation of titania nanoparticles and is correlated with the material photodarkening. Therefore, since the photoexcitation process results in the electron localization on Ti^{4+} center and hole transfer to organics, both organic and inorganic components of the hybrid material could contribute to the observed modification of refraction. The possible mechanisms are discussed below.

The photo induced modifications of refractive index in polymer are related to variation of density $\Delta\rho$ or of polarizability $\Delta\beta$, according to the Lorenz-Lorentz equation :

$$\frac{n^2 - 1}{n^2 + 2} = \frac{4\pi}{3} \rho \beta \tag{9}$$

Actually, a decreases of refractive index in silica-based organic-inorganic hybrid material under UV-light irradiation has been previously reported by Park et al. [23]. The effect was assigned to changes of the organic component polarizability resulting from the decomposition of methacryl chains and subsequent evaporation of carbonyl groups. In our case, the organic component of the hybrids is transparent in UV-A spectral region and cannot be decomposed by 375-nm photons. Moreover, the refraction modifications are reversible and no modification of volume sample has been observed after the irradiation. Therefore, the organic component may contribute to the refractive index variation only via a decrease of its polarizability as a result of the hole transfer from titania nanoparticles [10]. Indeed, the polarizability of -OEMA groups on the inorganic nanoparticle surface is explained by the mesomeric effect, as shown in Fig. 7 below:

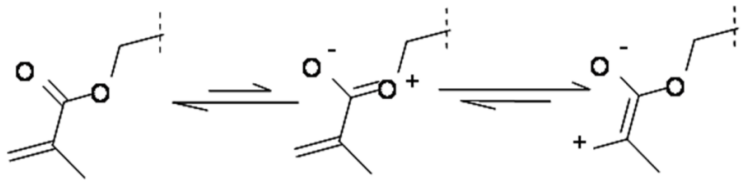

Fig 7: Charges distribution on -OEMA groups.

The presence of a double carbon bond in conjugation with a carboxylic group (α-position) may have a significant impact on the charges distribution when an electric field is applied. On the other hand, the hole transfer cancels the right-most configuration, which decreases the group polarizability. Although an exact place of the hole localization in not known, the organic polymerization is not complete in these hybrids [6,8] and non-polymerized -OEMA functional groups may remain at the organic-inorganic interface.

The origin of the refractive index reduction in semiconductors is usually assigned to the contribution of the free carriers conductivity by the so-called plasma effect [24]. Owing to the cw UV irradiation, free CB electrons permanently exist in our samples. Nevertheless, because of their short lifetime, they are not supposed to contribute significantly to the refractive index modification. This is confirmed by our experimental results. Indeed, the transmittance curves presented in Fig. 3 are independent of the UV laser intensity. Consequently, the observed refraction change cannot be directly related to the density of free CB electrons. Nevertheless, due to the presence of very long-lived (about weeks) photo-induced charges, the UV irradiated titania nanoparticles constituting the hybrids, may be considered as a n-doped semiconductor. Interestingly, the obtained values of the refractive index variation per Ti^{3+} center a_0 (table 1) are in the range $a_0 \approx -2.4(\pm 0.5) \cdot 10^{-23}\ cm^3$, which is in agreement with the

#180200 - $15.00 USD Received 2 Jan 2013; revised 7 Feb 2013; accepted 7 Feb 2013; published 1 Apr 2013

typical values reported for refractive index modifications induced by charge carriers in doped semiconductors [24]. In titania, CB electrons interact strongly with phonons and form small polarons Ti^{3+} centers [25]. In these conditions, the electron transport can be governed by hopping, where the electrons move between Ti atoms by thermal activation and/or tunneling processes [25, 26], over against the ballistic transport and Drude model description [27]. This polaronic conductivity could be responsible of the observed refractive index reduction. Experiments with hybrids materials prepared with different organic components should allow clarifying the contribution of organic and inorganic components to the refractive index change.

Finally, photoinduced permanent modifications of the refractive index have been reported in a large variety of materials as chalcogenide glass, oxide glass or polymers [8, 23, 28]. They are used to realize optical devices like wave guides, photonic structures, optical switches, etc …. Typical reported values of photoinduced refractive changes ranges from 10^{-4} to 10^{-1}. In the presented experiments the maximum refractive index modification $-5\cdot10^{-4}$ is found in sample X20 at the UV irradiation dose of 10 J/cm^2. Although, this value is sufficient to implement waves guide in our hybrids materials [29, 30], it's worth to remark that the Ti^{3+} concentration of the considered hybrid samples can attain 13% of the available Ti atoms [8,10]. Consequently, the photoinduced change of the refractive index could be much stronger. Assuming the refractive index change per Ti^{3+} center $a_0 \approx -2.4\,10^{-23}\ cm^3$, the maximum modification of the refractive index in sample X20 could attain $\Delta n_{0,max} \approx 0.005$. This estimation, which needs to be confirmed experimentally, makes the TiO_2-pHEMA hybrid material performance comparable with those of chalcogenide and oxide glasses. Moreover, the photopatterning in the hybrids is reversible, which may permit repetitive recording.

The present results indicate that the photosensibilty of our nanoparticulate hybrids is sensitive to the excitation photon energy: the quantum yield of charges separation attains 15% at 375 nm, which is considerably lower than previously reported 50% at 355 nm [13]. Moreover, the titania absorbance strongly increases with an increase of photon energy above bandgap of 3.24 eV (380 nm). Accordingly, photopatterning of the hybrids at the shorter wavelengths would increase of the structure contrast and process efficiency. We notice that the use in the present study of a laser diode emitted at 375 nm is explained by its perfect Gaussian spatial beamshape, essential for the refraction measurements.

The reproducibility of electronic properties of the hybrid materials requires a comment. In the present experiments, three series of hybrid samples with different inorganic concentrations ranging from X1 to X20 were tested, prepared of 5-nm titania nanoparticles and distillated HEMA monomer. We found that the quantum yield of the photoinduced charges separation depends sensitively on the surface state of glass plates, between which the hybrid is confined. In particularly using silica treated hydrophobic glass plates (instead of the not treated ones), the quantum yield of photoinduced charges separation can be increased by a factor of two, which can be explained by the titania adhesion to the glass surface. In the same time, the refraction factor a_0 remained in the range of $-2.4\cdot10^{-23}$ cm^3 irrespectively of the plates preparation (at the only exception of one sample X5 showed a_0 about twice higher, which may be related to the organic polymerisation extent that is beyond the scope of this communication). This confirms the photoinduced refraction relation to the created Ti^{3+} centers.

An almost constant value of a_0 reported in the Fig. 6 shows that the photoinduced refractive index modification per elementary e^-/h^+ pair excitation is not influenced by the inorganic nanoparticles concentration. This evidences the large organic/inorganic internal interface of these hybrids which is maintained until the highest nanoparticles loading (correspondent to the interparticles distance close to their size). The nanoparticulate hybrids

#180200 - $15.00 USD Received 2 Jan 2013; revised 7 Feb 2013; accepted 7 Feb 2013; published 1 Apr 2013

can be considered as open structure materials, which functional properties are defined by internal interface.

5. Conclusion

We report on measurements of photoinduced modifications of the linear optical refraction coefficient of nanoparticulate pHEMA-TiO_2 organic-inorganic hybrids at 375 nm. The samples with titania concentration ranging from 0.88×10^{20} (X1) to 17.6×10^{20} cm^{-3} (X20) were prepared and analyzed. The photoinduced phase shift was obtained from the evolution of the normalized on-axis sample transmittance as a function of the UV irradiation dose. The reduction of the refractive index with the increase of the UV irradiation dose was observed in all hybrids. The refraction per Ti^{3+} center $a_0 = \Delta n_0 / \left[Ti^{3+} \right] \approx -2.4 (\pm 0.5) \cdot 10^{-23}$ cm^3 was found almost independent on titania concentration. Both organic and inorganic components of the hybrid can contribute to the refractive changes. The strongest variation of $\Delta n = -5 \cdot 10^{-4}$ in the linear sample absorbance regime has been measured in X20 sample with the highest concentration of TiO_2 nanoparticles. At high irradiation doses close to the photodarkening saturation, the refraction index variations could attain -0.005, which makes these materials candidates for applications in optoelectronics.

#180200 - $15.00 USD Received 2 Jan 2013; revised 7 Feb 2013; accepted 7 Feb 2013; published 1 Apr 2013